applied sciences

MDPI

Article

Research on Nanometer Precision Measurement Method of High Order Even Aspheres

Hao Xu [1,2], Junfeng Liu [1,2] and Shanyong Chen [1,2,*]

[1] National Key Laboratory of Equipment State Sensing and Smart Support, College of Intelligence Science and Technology, National University of Defense Technology, Changsha 410073, China; haoxuxh@163.com (H.X.); ljf20090702122@163.com (J.L.)
[2] Hu'nan Key Laboratory of Ultra-Precision Machining Technology, Changsha 410073, China
* Correspondence: mesychen@163.com

Abstract: Optical aspheres are demanded with extremely high precision to meet functional requirements in space telescopes, extreme ultraviolet lithography, and other modern large optical systems. The nano-precision fabrication of optical aspheres requires high-precision measurements to guide deterministic optical processing. Null test is the preferred method for high-precision measurements. Null optics are required to compensate for the incident wavefront in the null test of optical aspheres. However, wavefront aberrations caused by the transmission flat or transmission sphere of interferometer and null optics can limit measurement accuracy and need to be separated. A nano-precision measurement method is proposed for the even optical aspheres of high order in this paper. A computer-generated hologram is used as a null optic to realize a null test on optical aspheres. Mapping distortion correction is performed on the measurement results to ensure that the transverse coordinates of the measurement results correspond correctly to those of the test surface. Absolute testing is applied to separate the wavefront aberrations caused by the computer-generated hologram and interferometer optics. Finally, the results obtained by this method were used to guide deterministic optical processing, enabling the nano-precision fabrication of optical aspheres.

Keywords: interferometry; null test; computer-generated holograms; optical aspheres

check for updates

Citation: Xu, H.; Liu, J.; Chen, S. Research on Nanometer Precision Measurement Method of High Order Even Aspheres. *Appl. Sci.* **2024**, *14*, 9969. https://doi.org/10.3390/app14219969

Academic Editor: Paolo Prosposito

Received: 25 September 2024
Revised: 22 October 2024
Accepted: 25 October 2024
Published: 31 October 2024

1. Introduction

Optical aspheres have the incomparable superiority of flats and spheres in improving image quality, correcting system aberration, and reducing system size and weight [1]. They have been widely used in large optical systems under extreme usage conditions, such as space telescopes [2], extreme ultraviolet lithography (EUVL) [3], and inertial confinement fusion (ICF) [4], to meet the functional requirements of the devices. Due to the mature development of ultra-precision machining technologies such as Magnetorheological Finishing (MRF) [5,6] and Ion Beam Figuring (IBF) [7–9], the surface shape accuracy of optical aspheres has been able to reach the nanometer scale. For example, the surface shape accuracy of projection optics for extreme ultraviolet lithography has been better than 0.1 nm [10]. Measurement results guide the deterministic optical processing, which means that machining accuracy is directly limited by that of measurement. Therefore, a precondition for realizing a breakthrough in the accuracy of surface shape is to improve the accuracy of measurement.

A number of methods have been used to achieve the high-accuracy measurements of optical aspheres, such as Sub-aperture Stitching Interferometry (SSI) and interferometry with compensators [11–17]. Sub-aperture Stitching Interferometry has enabled the high-precision measurements of non-rotationally symmetric optical freeforms and guided processing, resulting in the convergence of the error of freeform surface shape from 76 to 11 nm RMS [11]. Annular Sub-aperture Stitching Interferometry (ASSI) has been validated on steep aspheric and the measurement accuracy can reach the nanometer scale [12]. Using

a computer-generated hologram (CGH) as a null compensator can realize a null test of optical off-axis aspheres with high accuracy [13,14]. The mid-spatial frequency error of large aperture long-focal-length lenses can also be accomplished with high accuracy with the help of CGH and the RMS of the measurement results has reached the sub-nanometer level [15]. A novel SSI method based on monoscopic deflectometry has achieved the measurement of large aperture optical aspheres by rotating the measured mirror, and the system error has been calibrated [16]. The combination of SSI and the null compensator has completed the high-precision measurement of 320 mm large aperture optical asphere, realizing the null test of SSI [17]. Therefore, the null test is the preferred method to achieve the high-precision measurement of optical aspheres.

It is necessary to use absolute testing to separate the system error of interferometry when the accuracy of the test surface is comparable to that of the transmission flat (TF) or transmission sphere (TS). The two-sphere method, the three-flat test, the shift-rotation method, the N-position method, etc. are the commonly used absolute testing methods that are able to separate the system error to break through the measurement limits [18–22]. For example, eight rotation positions can be measured to separate the non-rotationally symmetric system errors of the lateral shearing interferometer [18]. The combination of the three-flat test and the N-position method has made it possible to measure large aperture optical flats up to 800 mm with nano-precision [20]. A new absolute testing method combining the even and odd function method and the three-flat test method is proposed, and with the help of a dedicated rotating device, in situ absolute testing can be realized on an interferometer with an aperture of 600 mm [21]. The combination of the N-position method and the random sphere method can separate the interferometer system error and the CGH error one by one, realizing the absolute testing of an optical asphere with an aperture of 300 mm, and the deformation due to fixture mounting and gravity is also taken into account [22]. Consequently, absolute testing is the key to pushing the limits of measurement accuracy.

In this paper, a high-precision measurement method applicable to even aspheres of high order is proposed to realize the null test with a CGH. Absolute testing is used to separate system errors and ultimately, the nano-scale precision measurement is realized. Techniques such as mapping distortion correction and image recognition are involved in the method proposed. The method of measurement is described in detail in Section 2. Experiments are carried out in Section 3 and the measurement results are obtained.

2. Methods

2.1. Null Compensation Interferometry with a CGH

The null test is the preferred method of optical measurement. For optical aspheres, null optics are required to achieve the null test. CGH is a commonly used compensator, which works like a diffraction grating with variable period and has curves in the pattern [23]. The phase of the incident wavefront passing through the CGH is modulated and transformed into a test wavefront that is consistent with the ideal surface shape of the test optical asphere, thus accomplishing the null test of the asphere. Therefore, the design of the phase function is crucial for a CGH to work properly and determines the diffraction pattern on the CGH. The diffraction pattern is a contour plot of the phase function intercepted according to a certain duty cycle. A single etched period on the diffraction pattern allows a phase modulation of the incident wavefront by 2 mπ where m is the order of diffraction. CGHs are categorized into amplitude-type and phase-type. Diffraction patterns on the substrate are created using raster scanning beam writing. A phase-type CGH is used in this paper and its phase distribution of the test hologram is shown in Figure 1. The design parameters of the test hologram are shown in Table 1.

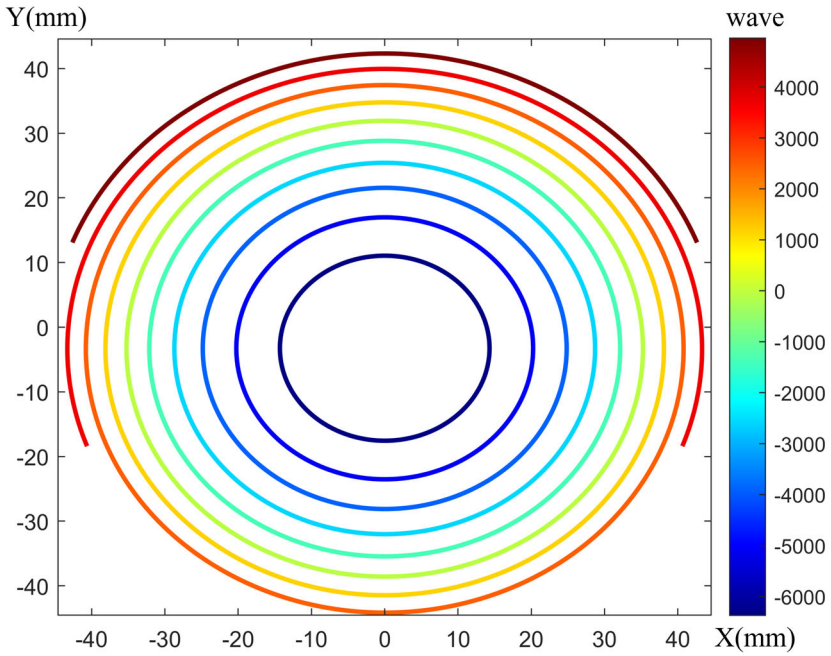

Figure 1. The phase distribution of the test hologram on the CGH.

Table 1. The design parameters of the test hologram.

Design Parameter	Setup	Design Parameter	Setup
Type	Phase-type	Average period	0.0073 mm
Size	89.2 mm	Carrier frequency	Tilt with 1.45°
Minimum period	0.0018 mm	Etching depth	0.5 μm
Maximum period	2.7045 mm	Duty cycle	0.5

A CGH often uses its +1 order diffraction for wavefront transform. However, other diffraction orders, such as 0 order, −1 order, etc., can have an effect on +1 order diffraction, creating ghost images in the interferometer and interfering with the measurement. Adding a carrier to the phase function of CGH to separate the other diffraction orders can effectively eliminate the effect of ghost images. Tilt carriers and power carriers are common choices [24,25]. A tilt carrier of 1.45° is applied to the CGH used in this paper to eliminate the effects of ghost images. Moreover, a pinhole with a radius of 3 mm is used to examine the ghost image in the Multi-Configuration of Zemax (v.2020), which shows that the applied tilt carrier eliminates the effect of other interfering diffraction orders.

Figure 2 shows the optical layout for the null test of an optical asphere with a CGH in this paper. In addition to the hologram used for the null test, alignment hologram and positioning hologram are also designed on the CGH [26,27]. The alignment hologram is used to adjust the relative position of the CGH to TF or TS. The positioning hologram is used to adjust the relative position of the test surface to the CGH. Although the diffractive structure period of CGH is larger at spherical wavefront incidence, the optical cavity length is too long in this case, which is about 500 mm. Consequently, a 6-inch TF is applied to produce parallel light incident on the CGH. The substrate of CGH is made of quartz with a certain thickness. When parallel light enters the substrate from the air, there is some distortion in the incident wavefront due to the change in refractive index. In order to eliminate the effects of substrate thickness and refractive index variations, the diffraction pattern was fabricated on the lower surface of the substrate. The optical layout of measurement and the CGH are designed in Zemax (v.2020).

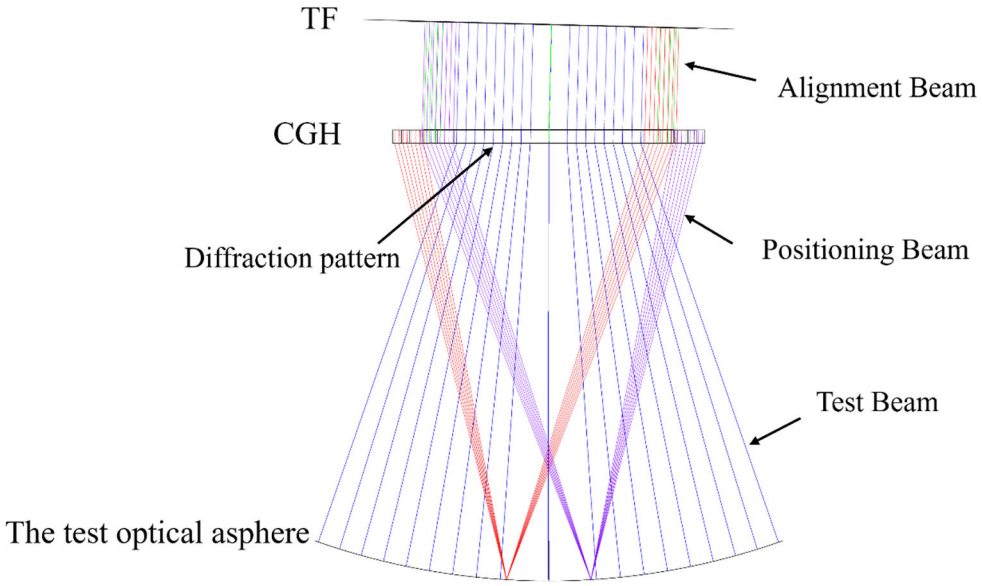

Figure 2. The optical layout of the optical asphere null test. The blue line represents the test beam. The red line and the purple line represent the positioning beam. The green line represents the alignment beam.

Parallel light selected as the incident wavefront is also intended to facilitate the subsequent calibration of the substrate error of the CGH by absolute testing using the same optical layout [28].

2.2. Correction of Mapping Distortion for the Result of Surface Shape

Mapping distortion often occurs in null tests on optical aspheres and freeforms. It is characterized by a nonlinear mapping of the transverse coordinates on the test surface to the transverse coordinates on the imaging surface of the interferometer. Mapping distortion is mainly caused by the incomplete imaging of light as it passes through the optics of the interferometer or null optics [29,30]. The occurrence of mapping distortion means that the image of the interferometer does not truly reflect the height distribution of the surface shape of the test surface in the transverse direction. That is unacceptable for high-precision deterministic processing, as the measurement result does not guide the process to accurate material removal at the exact location on the test surface. Consequently, it is necessary to correct the mapping distortion of the measurement results when using CGH for null tests on optical aspheres.

A pure ray tracing method is the mapping distortion correction method used in this paper. Dense rays are applied to trace the coordinate of the test surface to ensure that a sufficient number of feature points are used for correction. Since the transverse coordinates on the test surface and the imaging plane of the interferometer are not simply linearly proportional, we choose the TF as a transit surface in order to facilitate the calculation of the mapping relationship, as shown in Figure 3. Denote the coordinate of the point on the test surface as (x_t, y_t), the point on the CGH as (x_c, y_c), the point on the TF as (x_f, y_f), and the point on the imaging plane as (x_p, y_p).

Find two feature points (x_{p1}, y_{p1}) and (x_{p2}, y_{p2}) on the imaging plane, corresponding to (x_{t1}, y_{t1}) and (x_{t2}, y_{t2}) on the test surface, respectively. Then, (x_{f1}, y_{f1}) and (x_{f2}, y_{f2}) are the corresponding points on the TF traced through rays. The transverse coordinates on the TF are linearly related to those on the imaging plane by the following relationship:

$$a = \frac{\sqrt{\left(x_{f1} - x_{f2}\right)^2 + \left(y_{f1} - y_{f2}\right)^2}}{\sqrt{\left(x_{p1} - x_{p2}\right)^2 + \left(y_{p1} - y_{p2}\right)^2}} \tag{1}$$

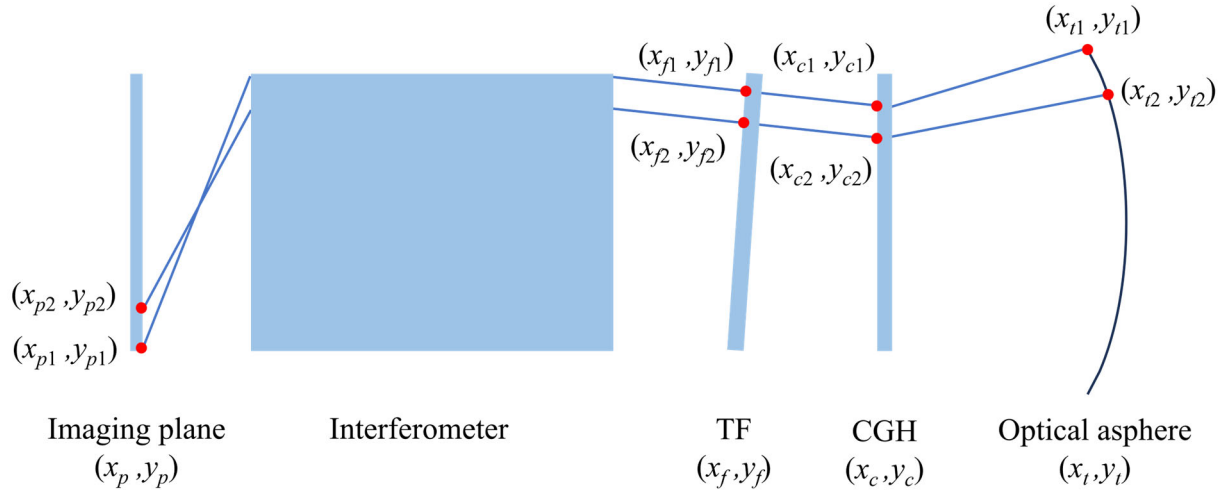

Figure 3. Tracing rays in mapping distortion correction.

Based on the relationship a, the coordinates of all the points on the TF corresponding to the imaging plane can be calculated as follows:

$$x_f = a(x_p - x_{p1}) + x_{f1} \tag{2}$$

$$y_f = a(y_p - y_{p1}) + y_{f1} \tag{3}$$

The tracing rays can be used to establish a one-to-one correspondence between the points on the test surface (x_f, y_f) and the points on the TF (x_t, y_t). At this point, the correspondence between the transverse coordinates of the points on the test surface and those of the points on the imaging plane has been successfully established. The tracing rays can be set dense enough to avoid a lack of fiducial marks. Finally, the correction is completed by using linear interpolation for data completion to form a complete error map in the height direction of the test surface. Zemax can be used to track the rays.

2.3. Absolute Testing of Optical Aspheres

Absolute testing can improve measurement accuracy down to the nanometer scale. An absolute testing method suitable for rotationally symmetric aspherical surfaces is used in this paper, which is a combination of the shift-rotation method and the N-position method. Details can be found in previous work [31].

The measurement result of the null test on an optical asphere with a CGH can be expressed as follows:

$$W(x,y) = W_R(x,y) + W_{CGH}(x,y) + W_T(x,y) \tag{4}$$

where $W_R(x,y)$ is the deviation of the reference surface, $W_{CGH}(x,y)$ is the wavefront aberration due to the CGH, and $W_T(x,y)$ is the surface shape of the test surface.

$$\begin{cases} W_1(\rho,\theta) = W_R(\rho,\theta) + W_{CGH}(\rho,\theta) + W_T(\rho,\theta) \\ W_2(\rho,\theta+\varphi) = W_R(\rho,\theta) + W_{CGH}(\rho,\theta) + W_T(\rho,\theta+\varphi) \\ \vdots \\ W_N(\rho,\theta+(N-1)\varphi) = W_R(\rho,\theta) + W_{CGH}(\rho,\theta) + W_T(\rho,\theta+(N-1)\varphi) \end{cases} \tag{5}$$

where $N = \frac{2\pi}{\varphi}$ and φ is the angle at which the test surface rotates around the optical axis each time.

A reverse rotation operation is performed on Equation (5), after which all the results are summed and averaged to obtain the following:

$$W_{aver}(x,y) = W_R^{sym}(x,y) + W_{CGH}^{sym} + W_T(x,y) \tag{6}$$

where W^{sym} is the rotationally symmetric component of the wavefront distortion.

Subsequently, the test asphere is replaced with a high-precision optical flat. Measurements at 4 positions are taken to calibrate the errors of the CGH and the reference surface. The results obtained are denoted as follows:

$$\begin{cases} W_1(x,y) = W_R(x,y) + W_{CGH}(x,y) + W_F(x,y) \\ W_2(\rho,\theta+\Delta\theta) = W_R(\rho,\theta) + W_{CGH}(\rho,\theta) + W_F(\rho,\theta+\Delta\theta) \\ W_3(x+\Delta x,y) = W_R(x,y) + W_{CGH}(x,y) + W_F(x+\Delta x,y) \\ W_4(x,y+\Delta y) = W_R(x,y) + W_{CGH}(x,y) + W_F(x,y+\Delta y) \end{cases} \tag{7}$$

where $W_F(x,y)$ is the surface shape error of the test optical flat, Δx is the distance of the test surface translated along the x-axis direction, Δy is the distance of the test surface translated along the y-axis direction, and $\Delta\theta$ is the angle of the test surface rotated about the optical axis.

Reverse the results of Equation (7) and subtract the last three terms from the first to obtain the following:

$$\begin{cases} W_2'(\rho,\theta) - W_1(\rho,\theta) = W_R(\rho,\theta-\Delta\theta) - W_R(\rho,\theta) + W_{CGH}(\rho,\theta-\Delta\theta) - W_{CGH}(\rho,\theta) \\ W_3'(x,y) - W_1(x,y) = W_R(x-\Delta x,y) - W_R(x,y) + W_{CGH}(x-\Delta x,y) - W_{CGH}(x,y) \\ W_4'(x,y) - W_1(x,y) = W_R(x,y-\Delta y) - W_R(x,y) + W_{CGH}(x,y-\Delta y) - W_{CGH}(x,y) \end{cases} \tag{8}$$

The surface shape is reconstructed by Zernike polynomials and the rotationally symmetric components are extracted as follows:

$$W_s^{sym}(x,y) = W_R^{sym}(x,y) + W_{CGH}^{sym}(x,y) \tag{9}$$

The absolute surface shape of the test asphere $W_T(x,y)$ can be obtained by subtracting Equation (6) from Equation (9).

3. Experiments and Results

3.1. Experimental Setup

The phase distribution and design parameters of the CGH used in the experiments have been described in detail in Section 2.1. The absolute testing experiments in this paper are performed in a 6-inch Zygo vertical interferometer working at 632.8 nm. A 6-inch TF is used as the lens. A 4-inch TF is applied as the high-precision optical flat to calibrate the system error of the CGH and interferometer. A piece of even optical asphere of high order with an aperture of 230 mm is used as the test surface.

The setup and optical layout of the N-position method of the optical asphere are shown in Figure 4. A high-precision rotation stage is used to realize the rotational transformation of the test surface around the optical axis.

The system error is calibrated by replacing the optical aspheric with a 4-inch TF with dimensions that satisfy the calibration of the test hologram for the CGH. The optical layout and the actual experimental setup are shown in Figure 5. Measurements need to be taken at 4 different positions to fulfill the requirements of the shift-rotation method. The high-precision rotation stage also works in this case.

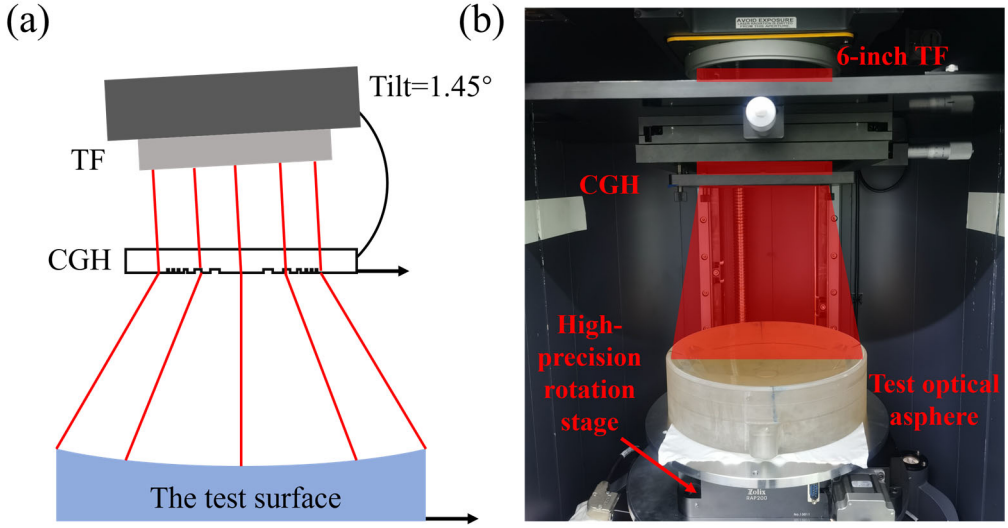

Figure 4. The setup of the optical asphere using the N-position method. (**a**) The optical layout. The red line represents the test beam and the arrow points in the direction of the original position; (**b**) the actual experimental setup.

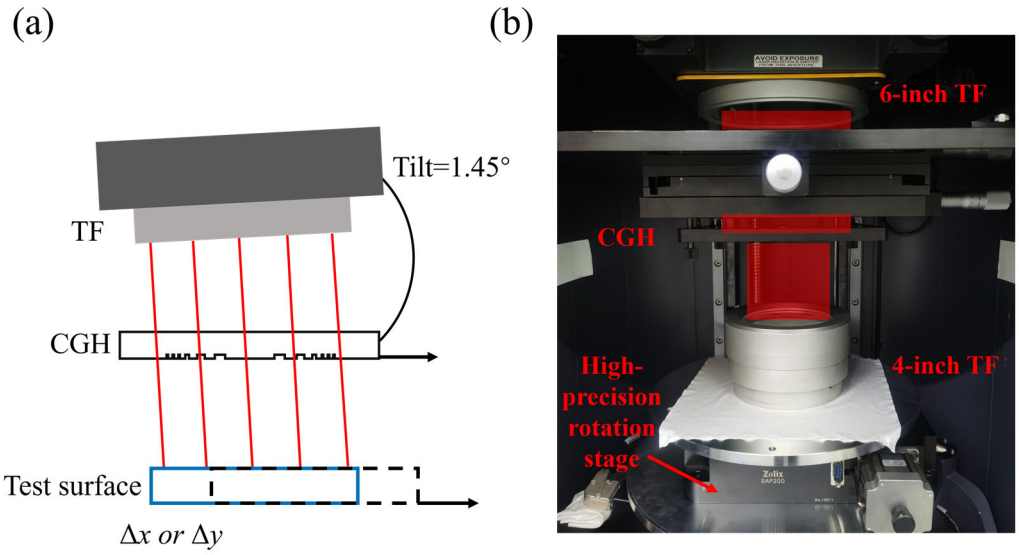

Figure 5. The setup of the high-precision flat using the shift-rotation method. (**a**) The optical layout. The red line represents the test beam and the arrow points in the direction of the original position; (**b**) the actual experimental setup.

3.2. Results and Discussion

In the initial stage of processing optical aspheres, turning and grinding are applied to complete the rough machining of the blank. After that, Single-Point Diamond Turning (SPDT), ultra-precision grinding, and other technologies are used to complete the finishing processing. At this stage, the RMS of the surface shape error of the optical asphere can converge from several wavelengths to within one wavelength. When interferometry is performed, the fringes can be very dense and make it difficult to analyze, resulting in incomplete measurement results. A non-contact profiler is a good choice to solve this problem, which can quickly and accurately measure the error of the surface shape of complex optical components. The non-contact profiler from DUI is employed to measure the surface shape of the optical asphere during the stage of MRF. The result is shown in Figure 6 and the uncertainty of measurement is within 15 nm.

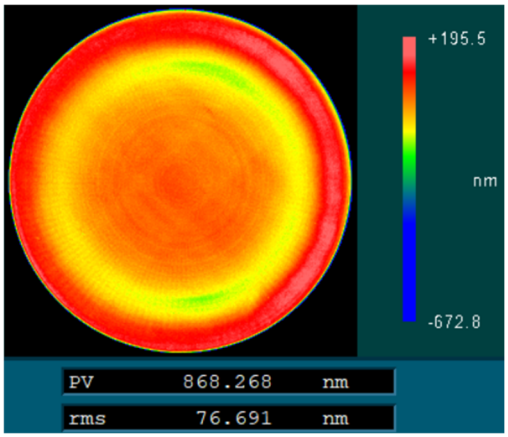

Figure 6. The measurement result of non-contact profiler.

With the gradual convergence of the RMS of the surface shape error, the optical asphere has to enter the stage of IBF. IBF accomplishes the accurate removal of material from a defined location on the surface. The accuracy of non-contact profilers is no longer sufficient to meet the requirements. The null test with CGHs is desired now, which is carried out in a 6-inch Fizeau interferometer that works at 632.8 nm. Mapping distortion can also affect the accuracy of material removal. The results before and after mapping distortion correction are shown in Figure 7, and mapping distortion correction is completed in Matlab (v.R2020b). It is clear that the PV and RMS of the surface shapes before and after correction have changed because the transverse coordinates of the imaging plane have been corrected and new data points have been generated by linear interpolation. The mapping profile looks similar before and after the distortion correction. That is because the test optical asphere is rotationally symmetric and the test hologram of the CGH used in the experiment is circular. No serious mapping distortion occurs when a plane wavefront passing through a test hologram becomes an aspherical wavefront.

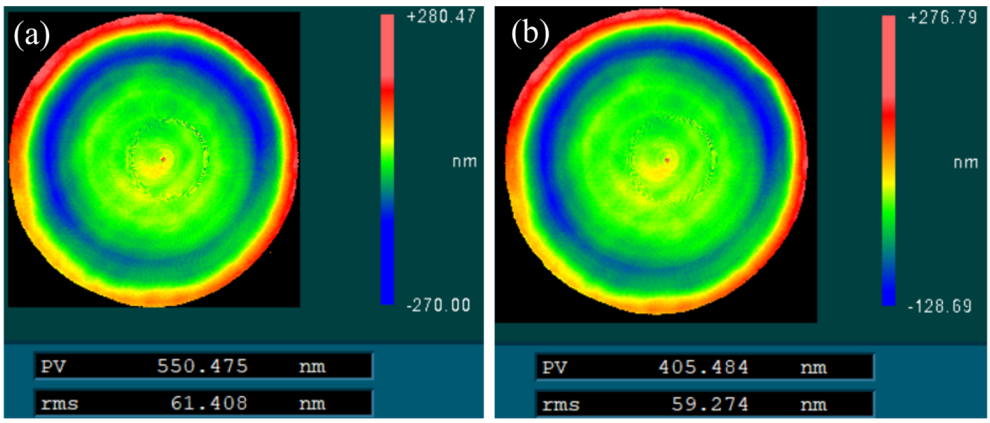

Figure 7. The results of the null test with a CGH before and after mapping distortion correction. (**a**) Before mapping distortion correction; (**b**) after mapping distortion correction.

The surface shape error of a TF PV is about λ/20, where λ is 632.8 nm. The RMS of the wavefront distortion caused by the CGH substrate used in this experiment is around 6 nm. When the surface shape error of the optical asphere converges to about 10 nm, the wavefront distortion caused by the TF and CGH can no longer be ignored. Absolute testing should be applied to separate errors. Two sets of absolute testing experiments have been carried out using the method described in Section 2.3. A 4-inch TF is applied as a high-precision optical flat to calibrate the error of the CGH and the 6-inch TF and measurement results of four positions (origin position, X-position, Y-position, and rotation position) are shown in Figure 8. It is clear that the results of the four positions do not vary

much. That is because the object that undergoes the position change is a 4-inch TF with a PV of about $\lambda/40$, which is more accurate than the system error.

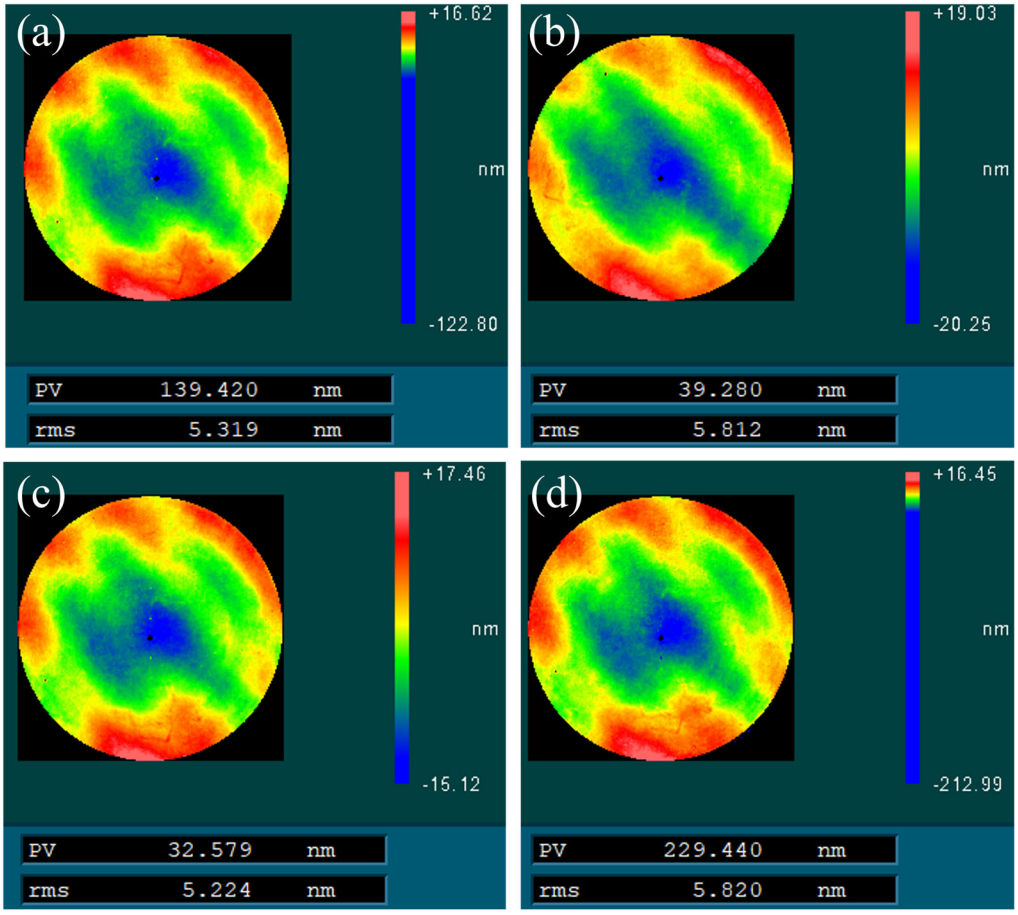

Figure 8. The results of the four positions of the 4-inch TF. (**a**) Origin position, (**b**) rotation position, (**c**) X-position, and (**d**) Y-position.

Image recognition is applied to determine the amount of translation of the 4-inch TF along either the x-axis direction or the y-axis direction. Three feature points are marked on the test surface and pictures are taken using the CCD of the interferometer. Feature points are identified by setting the gray scale thresholds and their coordinates are obtained in Matlab, as shown in Figure 9. Each time the test surface undergoes a translational transformation, feature points need to be set and their coordinates are recorded, as shown in Table 2. The effect on the absolute testing results is within 0.1 nm when the translation error is controlled within one pixel, which is shown in our previous work [31]. In the experiment of the shift-rotation method, Δx is 18.78 pixels, Δy is -17.70 pixels, and $\Delta\theta$ is 90°. In the experiment of the N-position method, φ is 30° and the test surface is measured 12 times. Figure 10 illustrates the results of the absolute testing of the optical asphere and the system error. Since the first 200 Zernike polynomials are used to process the measurements of the shift-rotation method, the results in Figure 10b obtained in Matlab lose some mid-frequency and high-frequency information compared to Figure 8. The results obtained by the method proposed in this paper guide IBF for deterministic material removal and the RMS of the surface shape error of the optical asphere converges to 4.85 nm, as shown in Figure 11.

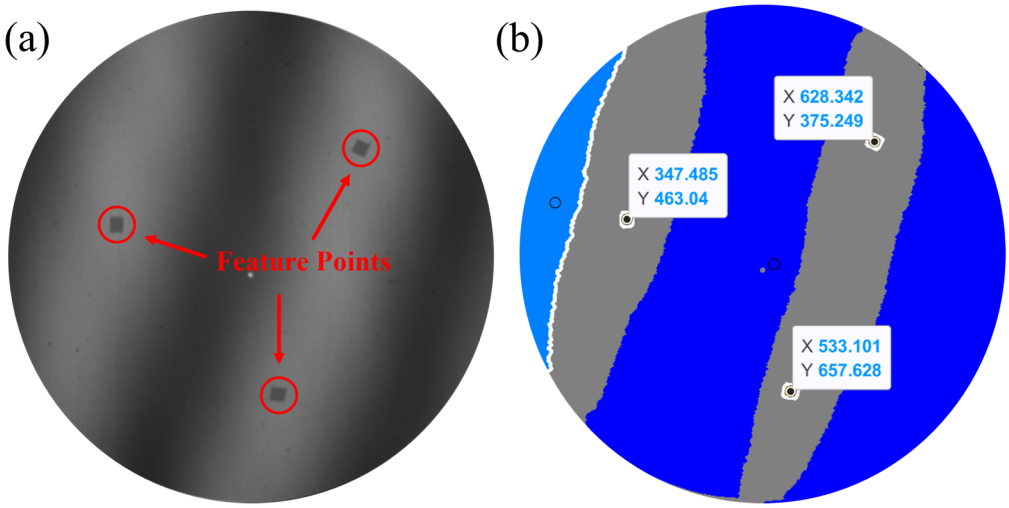

Figure 9. Image recognition of the coordinates of feature points. (**a**) Image of CCD; (**b**) coordinates of the feature points.

Table 2. Coordinates of the feature points at translation positions.

Unit: Pixels	X_1	Y_1	X_2	Y_2	X_3	Y_3	Average
Origin Position	347.48	463.04	628.34	375.25	533.10	657.63	
X-Position	328.50	463.12	609.75	375.17	514.30	657.65	
Δx	−18.98		−18.59		−18.80		−18.78
X–Y-Position	380.99	385.94	666.65	539.39	437.19	722.84	
Y-Position	381.09	368.29	666.55	521.90	437.13	704.89	
Δy		−17.65		−17.49		−17.95	−17.70

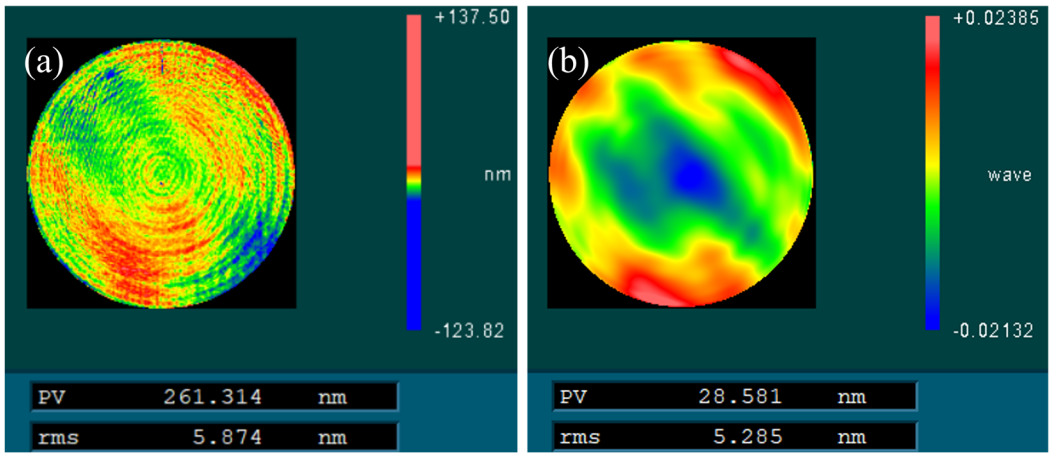

Figure 10. The results of the absolute testing of the optical asphere and the system error. (**a**) The result of the optical asphere with the N-position method, W_{aver}; (**b**) the result of the system error with the shift-rotation method, W_s.

In summary, the proposed method consists of four stages: non-contact profilometer measurement, null compensation interferometry with a CGH, mapping distortion correction, and absolute testing. The measurement results guided deterministic material removal and successfully converged the RMS of the surface shape error of the optical asphere from 76.69 to 4.85 nm, realizing the nano-precision manufacturing of optical aspheres. We have tried to keep the effect of each error on the results within 0.1 nm, such as noise, translation error, and rotation error. A detailed error analysis of the measurement process can be found in our previous work [31].

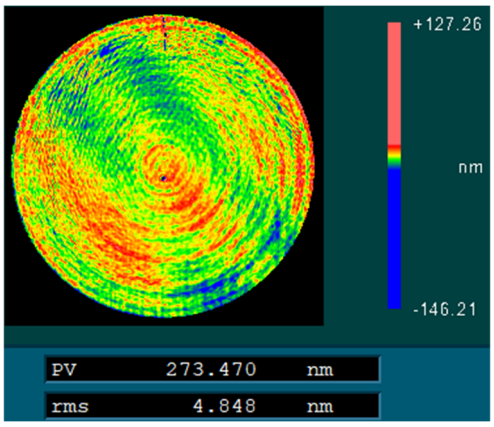

Figure 11. The absolute surface shape of the optical asphere obtained by the absolute testing method proposed in Section 2.3.

4. Conclusions

The accuracy of deterministic material removal processes, such as MRF and IBF, is limited by the accuracy of the measurements. The key to realizing the nano-precision manufacturing of optical aspheres is the improvement of measurement accuracy. In this paper, a nano-precision measurement method is proposed for even aspheres of high order. The method uses a combination of non-contact profiler and interferometry to achieve a measurement articulation during the surface shape accuracy of optical aspheres varying from low to high. The correction of mapping distortion ensures correct correspondence between the measurement results and the test surface shape in transverse coordinates, improving the accuracy of material removal. The null test of the optical asphere is accomplished by using a CGH as a null optic. Finally, the wavefront aberrations introduced by the CGH and TF are separated by absolute testing and the absolute surface shape of the optical asphere is obtained. The method proposed in this paper guided deterministic processing to converge the RMS of the surface shape error of the optical asphere from 76.69 to 4.96 nm, successfully realizing the nano-precision manufacturing of optical aspheres. A single measurement method can no longer be sufficient for monitoring the surface shape of optical elements during the entire process of manufacturing. The combination of contact and non-contact measurement, the combination of non-contact and null test, etc. has become more common in the measurement of optical components. The proposed method is also an example of the combination of different methods, along with the application of methods such as absolute testing and mapping distortion correction, which greatly improves measurement accuracy. This method is very effective in guiding the high-precision manufacturing of even optical aspheres of high order, and is expected to realize a breakthrough in the existing optical processing accuracy.

Author Contributions: Conceptualization, S.C. and H.X.; methodology, S.C.; software, H.X. and S.C.; validation, H.X., S.C. and J.L.; formal analysis, H.X. and S.C.; investigation, H.X., S.C. and J.L.; resources, H.X.; data curation, H.X.; writing—original draft preparation, H.X.; writing—review and editing, S.C.; visualization, H.X.; supervision, S.C. and J.L.; project administration, S.C. and J.L.; funding acquisition, S.C. and J.L. All authors have read and agreed to the published version of the manuscript.

Funding: The National Natural Science Foundation of China (No. 52375473 and No. 51991372).

Institutional Review Board Statement: Not applicable.

Informed Consent Statement: Not applicable.

Data Availability Statement: The raw data supporting the conclusions of this article will be made available by the authors upon request.

Conflicts of Interest: The authors declare no conflicts of interest.

References

1. Zhang, X.; Hu, H.; Wang, X.; Luo, X.; Zhang, G.; Zhao, W.; Wang, X.; Liu, Z.; Xiong, L.; Qi, E.; et al. Challenges and Strategies in High-Accuracy Manufacturing of the World's Largest SiC Aspheric Mirror. *Light Sci. Appl.* **2022**, *11*, 310. [CrossRef] [PubMed]
2. McElwain, M.W.; Feinberg, L.D.; Perrin, M.D.; Clampin, M.; Mountain, C.M.; Lallo, M.D.; Lajoie, C.-P.; Kimble, R.A.; Bowers, C.W.; Stark, C.C.; et al. The James Webb Space Telescope Mission: Optical Telescope Element Design, Development, and Performance. *PASP Publ. Astron. Soc. Pac.* **2023**, *135*, 058001. [CrossRef]
3. Zhang, Z.; Yan, J.; Kuriyagawa, T. Manufacturing Technologies toward Extreme Precision. *Int. J. Extrem. Manuf.* **2019**, *1*, 022001. [CrossRef]
4. Baisden, P.A.; Atherton, L.J.; Hawley, R.A.; Land, T.A.; Menapace, J.A.; Miller, P.E.; Runkel, M.J.; Spaeth, M.L.; Stolz, C.J.; Suratwala, T.I.; et al. Large optics for the national ignition facility. *Fusion Sci. Technol.* **2016**, *69*, 295–351. [CrossRef]
5. Liu, J.; Li, X.; Zhang, Y.; Tian, D.; Ye, M.; Wang, C. Predicting the Material Removal Rate (MRR) in Surface Magnetorheological Finishing (MRF) Based on the Synergistic Effect of Pressure and Shear Stress. *Appl. Surf. Sci.* **2020**, *504*, 144492. [CrossRef]
6. Liu, S.; Wang, H.; Zhang, Q.; Hou, J.; Zhong, B.; Chen, X. Regionalized Modeling Approach of Tool Influence Function in Magnetorheological Finishing Process for Aspherical Optics. *Optik* **2020**, *206*, 164368. [CrossRef]
7. Hu, J.; Hu, H.; Peng, X.; Wang, Y.; Xue, S.; Liu, Y.; Du, C. Multi-Dimensional Error Figuring Model for Ion Beams in X-Ray Mirrors. *Opt. Express* **2024**, *32*, 29458. [CrossRef]
8. Karabyn, V.; Polák, J.; Procháska, F.; Melich, R. Ion Beam Figuring with Using Einzel Lens. In Proceedings of the Optics and Measurement International Conference 2019, Liberec, Czech Republic, 8–10 October 2019; Kovačičinová, J., Ed.; SPIE: San Jose, CA, USA, 2019; Volume 11385, pp. 48–55.
9. Majhi, A.; Shurvinton, R.; Pradhan, P.C.; Hand, M.; Gu, W.; Da Silva, M.B.; Moriconi, S.; Nistea, I.; Alcock, S.G.; Wang, H.; et al. Sub-Nanometre Quality X-Ray Mirrors Created Using Ion Beam Figuring. *J. Synchrotron Radiat.* **2024**, *31*, 706–715. [CrossRef]
10. Lowisch, M.; Kuerz, P.; Conradi, O.; Wittich, G.; Seitz, W.; Kaiser, W. Optics for ASML's NXE:3300B Platform. In Proceedings of the Extreme Ultraviolet (EUV) Lithography IV, San Jose, CA, USA, 24–28 February 2013; Naulleau, P.P., Ed.; SPIE: San Jose, CA, USA, 2013; p. 86791H.
11. Supranowitz, C.; Lormeau, J.-P.; Maloney, C.; Murphy, P.; Dumas, P. Freeform Metrology Using Subaperture Stitching Interferometry. In Proceedings of the Optics and Measurement 2016 International Conference, Liberec, Czech Republic, 11–14 October 2016; Kovacicinova, J., Ed.; SPIE: San Jose, CA, USA, 2016; p. 101510D.
12. Zhang, L.; Tian, C.; Liu, D.; Shi, T.; Yang, Y.; Wu, H.; Shen, Y. Non-Null Annular Subaperture Stitching Interferometry for Steep Aspheric Measurement. *Appl. Opt.* **2014**, *53*, 5755. [CrossRef]
13. Li, S. A Practical Method for Determining the Accuracy of Computer-Generated Holograms for off-Axis Aspheric Surfaces. *Opt. Lasers Eng.* **2016**, *77*, 154–161. [CrossRef]
14. Li, S.; Zhang, J.; Liu, W.; Liang, H.; Xie, Y.; Li, X. The methods and experiments of shape measurement for off-axis conic aspheric surface. *Materials* **2020**, *13*, 2101. [CrossRef] [PubMed]
15. Cui, J.-P.; Zhang, N.; Liu, J.; Wu, D.-L.; Xu, H.; Yan, D.-Y.; Ma, P. Testing the Mid-Spatial Frequency Error of a Large Aperture Long-Focal-Length Lens with CGH. *Opt. Express* **2020**, *28*, 9454–9463. [CrossRef] [PubMed]
16. Chen, T.; Chen, Y.; Lang, W.; Zhang, X.; Wang, W.; Xu, M. In-Situ Sub-Aperture Stitching Measurement Based on Monoscopic Phase Measuring Deflectometry. *Precis. Eng.* **2024**, *85*, 197–204. [CrossRef]
17. Li, Y.; De, Z.; Xue, Z.; Ming, L.; Xiao, W.; Dong, M. Experimental study on hybrid compensation testing of an off-axis convex ellipsoid surface. *Opt. Express* **2019**, *27*, 27546–27561.
18. Zhang, L.; Qi, K.; Xiang, Y. Two-step algorithm for removing the rotationally asymmetric systemic errors on grating lateral shearing interferometer. *Opt. Express* **2018**, *26*, 14267–14277. [CrossRef]
19. Liu, Y.; Miao, L.; Zhang, W.; Jin, C.; Zhang, H. Extended Shift-Rotation Method for Absolute Interferometric Testing of a Spherical Surface with Pixel-Level Spatial Resolution. *Appl. Opt.* **2017**, *56*, 4886. [CrossRef]
20. Ma, Z.; Chen, L.; Ma, J.; Zheng, D.; Zhang, Z.; Liu, Y. Absolute Tests of Three Flats for Interferometer with 800 Mm Aperture. *Opt. Express* **2024**, *32*, 3779. [CrossRef]
21. You, Z.; Shi, L.; Qi, L.; Yun, B.; Fu, W.; Jian, S. In situ absolute surface metrology for a 600 mm aperture interferometer. *Opt. Lasers Eng.* **2020**, *129*, 106054.
22. Wei, L.; Shenq, C.; Chen, H.; Ching, K.; Chien, C.; Wei, H.; Shih, T.; Cheng, S. Absolute measurement method for correction of low-spatial frequency surface figures of aspherics. *Opt. Eng.* **2017**, *56*, 055101.
23. Chen, S.; Xue, S.; Zhai, D.; Tie, G. Measurement of Freeform Optical Surfaces: Trade-Off between Accuracy and Dynamic Range. *Laser Photonics Rev.* **2020**, *14*, 1900365. [CrossRef]
24. Peng, J.; Ren, J.; Zhang, X.; Chen, Z. Analytical Investigation of the Parasitic Diffraction Orders of Tilt Carrier Frequency Computer-Generated Holograms. *Appl. Opt.* **2015**, *54*, 4033. [CrossRef]
25. He, Y.; Hou, X.; Wu, F.; Ma, X.; Liang, R. Analysis of Spurious Diffraction Orders of Computer-Generated Hologram in Symmetric Aspheric Metrology. *Opt. Express* **2017**, *25*, 20556. [CrossRef] [PubMed]
26. Xu, H.; Lu, W.; Chen, S. Positioning of the Test Surface in a CGH Null Test by Cat's Eye Interference. *Opt. Lasers Eng.* **2025**, *184*, 108627. [CrossRef]
27. Wang, X.; Liu, Z.; Su, H.; Cheng, Q.; Li, L.; Li, F. Mixed Compensation for the Testing of Large Convex Aspheres. *Results Phys.* **2023**, *55*, 107189. [CrossRef]

28. Zhou, P.; Burge, J.H. Fabrication Error Analysis and Experimental Demonstration for Computer-Generated Holograms. *Appl. Opt.* **2007**, *46*, 657. [CrossRef]
29. Hayden, J.E.; Lewis, T.S. Distortion Correction Method for Aspheric Optical Testing. In Proceedings of the Laser Interferometry X: Techniques and Analysis, San Diego, CA, USA, 30 July–4 August 2000; Kujawinska, M., Pryputniewicz, R.J., Takeda, M., Eds.; SPIE: San Diego, CA, USA, 2000; pp. 56–62.
30. Novak, M.; Zhao, C.; Burge, J.H. Distortion Mapping Correction in Aspheric Null Testing. In Proceedings of the Interferometry XIV: Techniques and Analysis, San Diego, CA, USA, 10–14 August 2008; Schmit, J., Creath, K., Towers, C.E., Eds.; SPIE: San Diego, CA, USA, 2008; p. 706313.
31. Xu, H.; Lu, W.; Luo, G.; Wang, Y.; Liu, Y.; Chen, S.; Liu, J. Absolute Testing of Rotationally Symmetric Surfaces with Computer-Generated Holograms. *Opt. Express* **2024**, *32*, 31055. [CrossRef]